Mesoporous Cobalt Molybdenum Nitride: A Highly Active Bifunctional Electrocatalyst and Its Application in Lithium−O2 Batteries

ARTICLE *in* THE JOURNAL OF PHYSICAL CHEMISTRY C · JANUARY 2013

Impact Factor: 4.77 · DOI: 10.1021/jp310571y

THE JOURNAL OF PHYSICAL CHEMISTRY C

Article

pubs.acs.org/JPCC

Mesoporous Cobalt Molybdenum Nitride: A Highly Active Bifunctional Electrocatalyst and Its Application in Lithium−O_2 Batteries

Kejun Zhang,[†,‡,∥] Lixue Zhang,[†,∥] Xiao Chen,[†] Xiang He,[§] Xiaogang Wang,[†] Shanmu Dong,[†] Pengxian Han,[†] Chuanjian Zhang,[†,‡] Shan Wang,[†,‡] Lin Gu,[§] and Guanglei Cui[†,*]

[†]Qingdao Institute of Bioenergy and Bioprocess Technology, Chinese Academy of Sciences, Qingdao 266101, China

[‡]University of Chinese Academy of Sciences, Beijing, 100039, China

[§]Beijing National Laboratory for Condensed Matter Physics, Institute of Physics, Chinese Academy of Sciences, Beijing 100080, China

Supporting Information

ABSTRACT: Bifunctional electrocatalysts for the oxygen reduction reaction (ORR) and the oxygen evolution reaction (OER) play a critical role in fuel cells and metal−air batteries. In this article, mesoporous cobalt molybdenum nitride (Co_3Mo_3N) is prepared using a coprecipitation method followed by ammonia annealing treatment. Much more active sites generated by well designed mesoporous nanostructure and intrinsically electronic configuration lead to excellent electrocatalytic performance for ORR/OER in Li−O_2 cells, delivering considerable specific capacity and alleviating polarization. It is manifested that high charge−discharge efficiency and good cycle stability were obtained in the LiTFSI/TEGDME electrolyte owing to a stable interface between optimized electrolyte and electrode material.

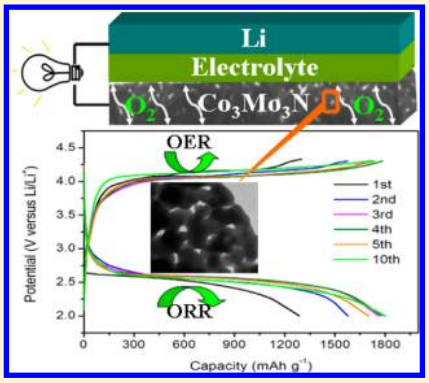

INTRODUCTION

The rechargeable nonaqueous Li−O_2 batteries are generating a great deal of interest due to their high theoretical energy density, which is much higher than state-of-the-art lithium-ion batteries.[1−5] This high energy density endows Li−O_2 batteries with great promise for high energy storage applications. However, Li−O_2 batteries still suffer from mainly the cyclability of triple-phase interface among electrolyte, catalyst, and oxygen owing to the interfacial reaction on oxygen electrode. A typical nonaqueous Li−O_2 battery consists of a lithium−metal anode, the organic electrolyte, and a porous carbon-based cathode exposed to gaseous O_2 during cell operation.[6−8] During discharge/charge processes, the sluggish kinetics of oxygen reduction/evolution reactions (ORR/OER) not only increases the overpotential by polarization, but also causes poor cycle efficiency. On the other hand, the solid discharge products are insoluble and thus precipitate in the pores of cathode, which gradually block the catalytic sites as well as the diffusion pathways of electrolyte and oxygen, and eventually degrade the performance of Li−O_2 batteries. It is well-known that nanostructured electrocatalysts can make a significant reduction in overpotential and energy consumption, due to the increased active sites and the reduced current density derived from the high surface area.[9] Thus, it is quite critical to develop effective catalysts with porous structure to facilitate the ORR/OER for Li−O_2 batteries.

Recently, a variety of electrocatalysts for Li−O_2 batteries have been explored.[4] Especially, bifunctional catalysts, such as Pt/Au nanoparticles,[10] α-MnO_2/Pd,[11] $MnCo_2O_4$/GNS,[12] and $CoMn_2O_4$/GNS[13] have been extensively investigated due to their attractive properties, most of these work used carbonate based electrolytes, which are frequently used in the present nonaqueous Li−O_2 cells.[10−13] However, the degradation of carbonate electrolytes is too severe to act as stable electrolytes of Li−O_2 battery.[14−16] It has been reported that ether solvents are much more stable than carbonate electrolytes as the electrolytes of Li−O_2 battery, and the discharge product is mainly Li_2O_2 or Li_2O.[17−22] Although much progress has been achieved, it still remains a great challenge to explore novel bifunctional electrocatalysts to upgrade the performance of Li−O_2 cells by lowering the overpotential and improving cycle life.

Transition bimetallic nitrides have exhibited interesting mechanical, electronic, optical and catalytic properties.[23−27] One of the primary interests for exploring transition bimetallic nitrides is to replace group VIII noble metals with low cost alternative metals. It is deduced that ternary nitrides can effectively tune the electronic configuration and thus regulate the catalytic activity relative to their binary constituents.[28,29]

Received: October 25, 2012
Revised: December 18, 2012
Published: December 18, 2012

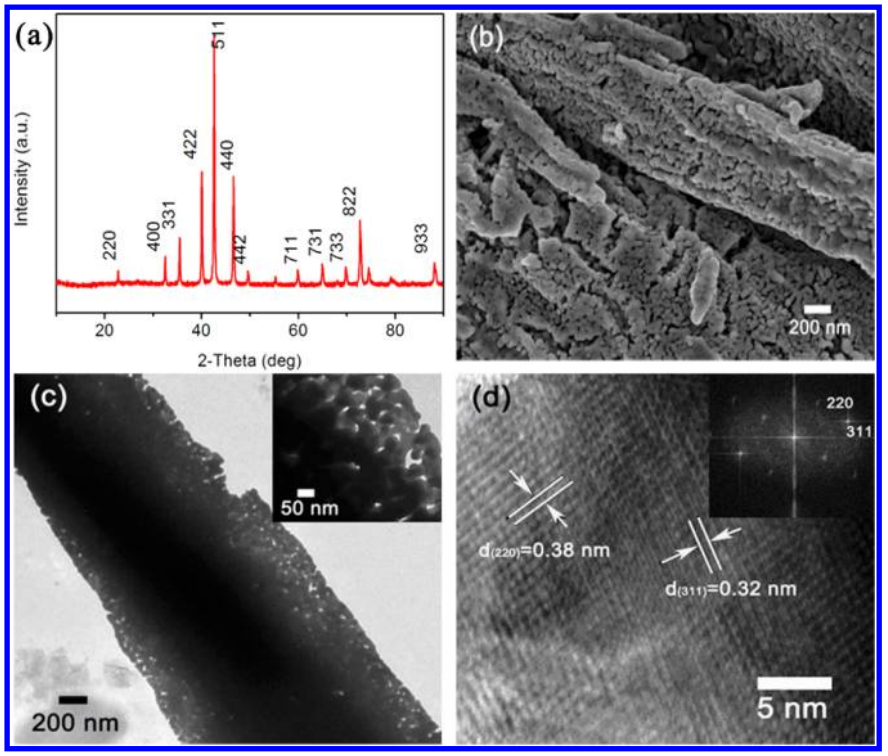

Figure 1. (a) Typical XRD pattern of Co_3Mo_3N. (b) SEM image of Co_3Mo_3N. (c) TEM images of Co_3Mo_3N. (d) HRTEM image and the corresponding FFT patterns (inset) of Co_3Mo_3N.

Among the numerous varieties of transition bimetallic nitrides, the η-carbide structured ternary molybdenum nitride (Co_3Mo_3N) shows significantly higher catalytic activity for ammonia synthesis than molybdenum nitride (MoN).[30−32] Jacobsen and co-workers[33] have explained the higher activity of Co_3Mo_3N derived from the combination of Co (with weak binding energy) and Mo (with strong binding energy) with nitrogen, which produced an alloy with an optimum nitrogen binding energy. MoN has been reported to exhibit a high activity in nonaqueous Li−O_2 batteries.[34,35] These studies inspire us to investigate the electrocatlytic activity of Co_3Mo_3N toward ORR/OER and explore Co_3Mo_3N-based catalyst for Li−O_2 battery cathode, since the introduction of cobalt element into MoN might regulate the affinity of oxygen to the transition bimetallic nitrides and thus improve its electrocatalytic activity.

In this article, mesoporous Co_3Mo_3N was synthesized and used as electrocatalyst in nonaqueous Li−O_2 batteries. The detailed characterization shows that Co_3Mo_3N possesses intriguing bifunctional electrocatalytic capability for ORR/OER in aqueous solution. When Co_3Mo_3N was employed as cathode catalyst, the Li−O_2 battery manifests lower anodic overpotential and an excellent cycle performance. This promising performance should be attributed to the intrinsically high catalytic activity and the unique structure, indicating that Co_3Mo_3N is a promising cathode catalyst candidate for Li−O_2 battery application.

EXPERIMENTAL SECTION

Synthesis of Co_3Mo_3N Catalyst. The Co_3Mo_3N was prepared by nitriding a cobalt molybdate hydrate ($CoMoO_4$) precursor,[29] which was prepared by adding ammonium heptamolybdate ($(NH_4)_6Mo_7O_{24}\cdot 4H_2O$, 2 g) to the aqueous solutions (100 mL) of cobalt nitrate ($Co(NO_3)_2\cdot 6H_2O$, 2.8 g) and heating the mixed solution to approximately 80 °C. The purple precipitate, $CoMoO_4\cdot nH_2O$, was washed twice with distilled water and once with ethanol and then dried overnight at 120 °C. The powder was then calcined at 500 °C for 3 h in air. $CoMoO_4$ was calcined in a tubular furnace at 800 °C under ammonia for 5 h with a progressive, slow heating ramp (room temperature to 350 °C, 5 °C min^{-1}; 350 to 450 °C, 0.5 °C min^{-1}; 450 to 800 °C, 2 °C min^{-1}). The sample was subsequently cooled to ambient temperature in the ammonia flow. To prevent potential bulk oxidation on exposure of the nitrided material to air, the material was passivated using a gas mixture containing 0.1% O_2 (N_2, 99%).

Catalyst Characterization. X-ray diffraction (XRD) pattern was recorded in a Bruker-AXS Microdiffractometer (D8 ADVANCE) from 10 to 85°. The morphology of the Co_3Mo_3N was attained from field emission scanning electron microscopy (FESEM, HITACHI S-4800), high-resolution transmission electron microscopy (TEM, JEOL 2010F). N_2 adsorption−desorption measurements were carried out at 77 K using a Quantachrome Autosorb gas-sorption system. X-ray photoelectron spectroscopy (XPS) was acquired using an ESCALab220i-XL spectrometer (VG Scientific) with Al Kα radiation in twin anode at 14 kV × 16 mA. Fourier transform infrared (FTIR) measurements were obtained on a JASCO FT/IR-6200 instrument from 2000 to 400 cm^{-1} with a resolution of 2 cm^{-1}. The ^1H NMR and ^{13}C NMR spectra were recorded on a 600 MHz NMR spectrometer (Bruker AVANCE III 600).

Electrochemical Characterization. Linear scanning voltammogram data were collected with a CHI 440 electrochemical workstation. A 5 mg sample of Co_3Mo_3N was dispersed in a mixture of 950 μL of deionized water and 50 μL of Nafion to prepare a homogeneous ink, a 5 μL drop of ink was put onto a 0.07 cm^2 glassy-carbon disk electrode and dried at room temperature. A Ag/AgCl electrode and a platinum wire

dx.doi.org/10.1021/jp310571y | J. Phys. Chem. C 2013, 117, 858−865

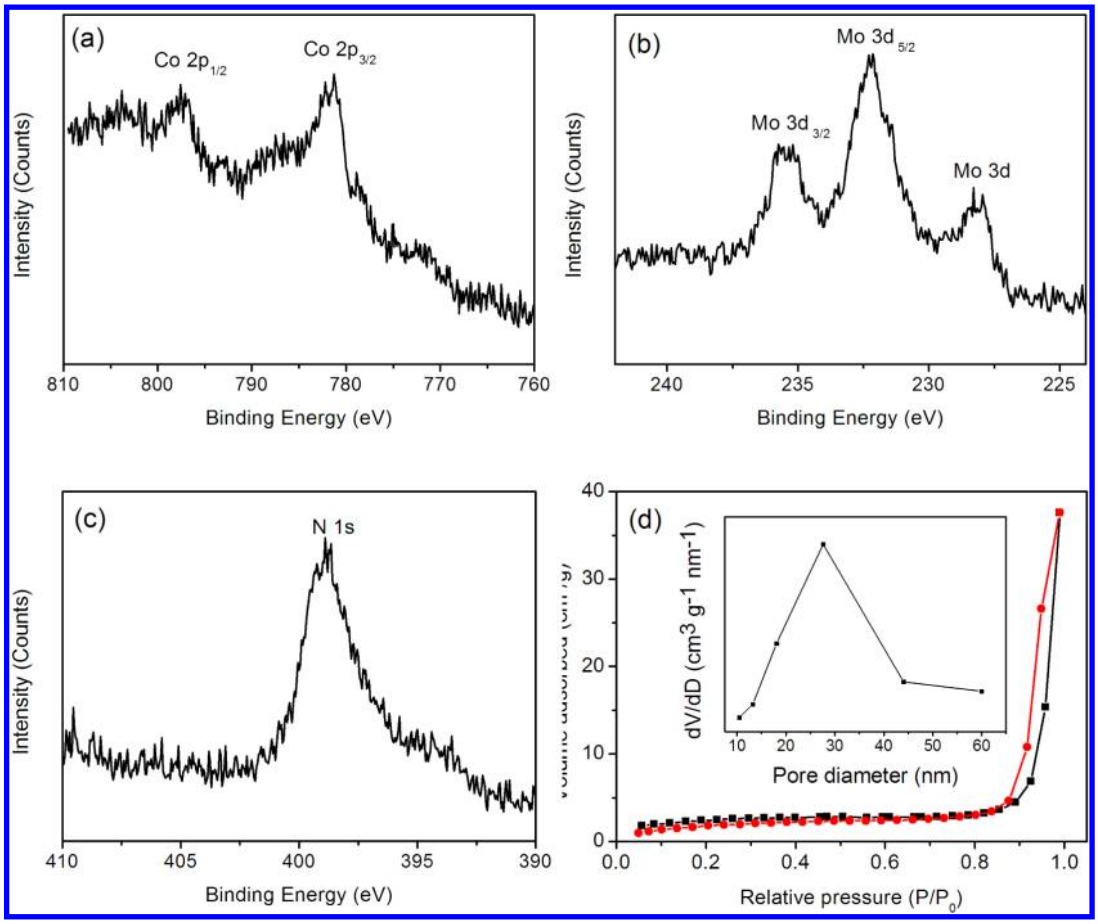

Figure 2. (a) Co 2p XPS spectrum of Co_3Mo_3N. (b) Mo 3d XPS spectrum of Co_3Mo_3N. (c) N 1s XPS spectrum of Co_3Mo_3N. (d) Nitrogen adsorption−desorption isotherms of Co_3Mo_3N and the pore-size distributions.

were used as the reference and counter electrodes, respectively. The electrolyte is 0.1 M aqueous KOH. The linear sweep voltammetry was obtained at a scan rate of 10 mV s^{-1} in the potential range −0.6 to +0.2 V (ORR) or 0.5−1.0 V (OER).

Li−O_2 cells consisted of a lithium metal anode and an air electrode of Co_3Mo_3N or pure super P. The O_2 electrodes (typically 1.0 mg) were prepared by mixing 40 wt % Co_3Mo_3N with 40 wt % super P and 20 wt % polytetrafluoroethylene (PTFE) binders, or 70 wt % super P with 30 wt % PTFE. The samples were rolled into slices and cut into square pieces of 0.5 cm ×0.5 cm, then pasted on a stainless steel current-collector under a pressure of 5 MPa. Electrochemical experiments were carried out by using a swagelok cell with a hole drilled only on the cathode of current collector to enable oxygen flow in. The Li−O_2 cells were assembled inside the glovebox under argon atmosphere (<1 ppm H_2O and O_2) by using a clean lithium metal disk (8 mm diameter) as anode, a glass-fiber and a polypropylene (Celgard 2400) as separators, 1 M LiTFSI in TEGDME as electrolyte. Galvanostatical discharge−charge experiments were tested on a LAND battery testing system. The capacity was calculated based on the total mass of the oxygen electrode (electrocatalyst + carbon + binder).

RESULTS AND DISCUSSION

The preparation of Co_3Mo_3N mainly consists of two steps: the synthesis of $CoMoO_4$, and the successive synthesis of mesoporous Co_3Mo_3N transformed from $CoMoO_4$ precursor under ammonia atmosphere. The formation of $CoMoO_4$ is confirmed by XRD experiment (Figure S1 in the Supporting Information), and the SEM experiment shows an irregular microstructure of $CoMoO_4$ (Figure S2, Supporting Information). Then, after the following pretreatment, ammonolysis and passivation treatments in ammonia atmosphere, the well-crystallized Co_3Mo_3N was obtained. The as-prepared nitrided product was investigated by conventional XRD experiment, as shown in Figure 1a. All the peaks match the reference data of a pure Co_3Mo_3N phase.[30] The SEM image in Figure 1b shows that there are many pores exist in Co_3Mo_3N microstructure. From the TEM image (Figure 1c), a microstructure with many mesopores in the diameters between 10 and 40 nm was observed. The microstructure of the product was further investigated by the HRTEM (Figure 1d), indicating the well crystallinity of the synthesized Co_3Mo_3N. The measured neighboring interlayer distance is consistent with the spacings of the (220) and (311) phases of cubic Co_3Mo_3N. The well-defined points in the FFT pattern also agree well with the allowed Brag diffraction of cubic Co_3Mo_3N.

XPS measurements were performed to analyze the chemical composition of Co_3Mo_3N. As shown in Figure 2a-2c, the Co (2p), Mo (3d) and N (1s) peaks confirmed the presence of each element. The N_2 adsorption−desorption isotherm and the pore-size distributions derived from the adsorption isotherms for Co_3Mo_3N are shown in Figure 2d. The isotherm of Co_3Mo_3N exhibits the characteristics of type IV, and the H1 hysteresis loop is the indicative of mesoporosity. The pore-size distribution (10−40 nm) is also well agreement with the SEM

dx.doi.org/10.1021/jp310571y | J. Phys. Chem. C 2013, 117, 858−865

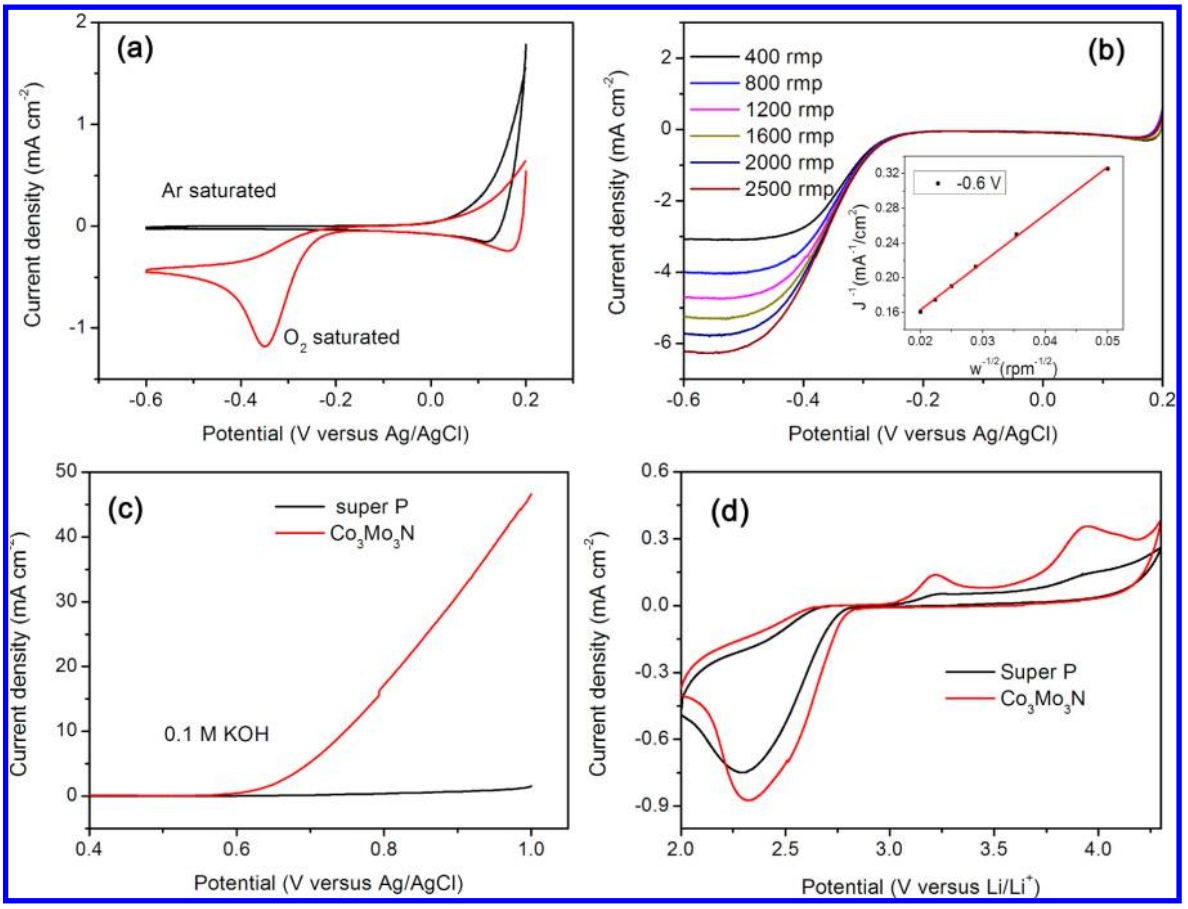

Figure 3. (a) Cyclic voltammetry curves of ORR for Co_3Mo_3N-modified electrode. (b) Linear sweep voltammetry curves of ORR at various rotation rates for Co_3Mo_3N-modified electrode, inset is the corresponding K–L plots. (c) Oxygen evolution curves for Co_3Mo_3N and super P modified electrodes measured in 0.1 M KOH. (d) CV curves of super P and Co_3Mo_3N-based electrode in TEGDME electrolyte containing 1 M LiTFSI at a scan rate of 0.05 mV s^{-1}.

and TEM results. It is reasonable that these mesopores can deliver a shorter ion transport pathway and more triple-phase (solid–liquid–gas phases) regions required for oxygen reduction.

Most of the catalysts used in nonaqueous Li–O_2 batteries in literatures are those materials that have already been proven to be efficient catalysts for ORR/OER in aqueous phase.[5,10,12,13] Therefore, the electrocatalytic activity of Co_3Mo_3N toward ORR and OER in aqueous was evaluated by electrochemical approaches. Figure 3a shows the CVs of Co_3Mo_3N in 0.1 M KOH saturated with either argon or oxygen at a potential scan rate of 0.01 V s^{-1}. Compared with the featureless CV profile in Ar-saturated electrolyte, a strong reduction current peak can be observed when the electrolyte was saturated with O_2, suggesting the electrocatalytic activity of the as-synthesized Co_3Mo_3N toward oxygen cathodic reduction. Rotating-disk electrode technique was carried out to further investigate the electrocatalytic ORR behavior of Co_3Mo_3N (Figure 3b). From the slope of corresponding Koutecky–Levich plot (Inset in Figure 3b),[13] the electron transfer number (n) per O_2 molecule is evaluated to be 3.8 for the Co_3Mo_3N modified-electrode. These results suggest an apparent quasi-four-electron process, which is desirable for achieving highly efficient electrocatalytic ORR. An ideal catalyst for a rechargeable Li–O_2 battery needs to have not only ORR activity, but also good OER activity. The electrocatalysis toward OER with Co_3Mo_3N, pure super P and MoN were investigated (Figure 3c and Figure S4, Supporting Information). Co_3Mo_3N-modified electrode shows a much higher catalytic activity toward OER than pure super P and MoN-modified electrodes. This result is consistent with the previous X-ray absorption near-edge structure (XANES) observations that the Co ions was considered to be the active sites for OER.[36] Such a remarkable OER activity of Co_3Mo_3N might be adopted to lower the charging polarization in Li–O_2 battery.

To explore the application of the Co_3Mo_3N in nonaqueous electrolyte, CV of Li–O_2 batteries with Co_3Mo_3N and super P are obtained in TEGDME electrolyte containing 1 M LiTFSI at a scan rate of 0.05 mV s^{-1}. As shown in Figure S5 (Supporting Information) and Figure 3d, featureless CV curve of Co_3Mo_3N is observed in the Ar-saturated solution, while in the O_2-saturated solution, Co_3Mo_3N electrode exhibits a slightly higher ORR onset potentials and higher ORR peak current than super P electrode. In the anodic scan, Co_3Mo_3N electrode exhibits a slightly lower OER onset potential and higher OER peak currents than super P electrode. It is noted that the Co_3Mo_3N electrode contains 40% super P and possesses an alleviated surface area of Co_3Mo_3N electrode over Super P electrode (Super P, 62 m^2/g; Co_3Mo_3N, 16 m^2/g). These two anodic peaks should be attributed to the oxidation of LiO_2 and Li_2O_2 respectively.[37,38] This result suggests that Co_3Mo_3N has considerable ORR/OER catalytic activity in nonaqueous Li–O_2 batteries rather than an artifact of differences in electrode surface area.

dx.doi.org/10.1021/jp310571y | J. Phys. Chem. C 2013, 117, 858–865

The performance of the Co_3Mo_3N for ORR/OER in Li−O_2 batteries was evaluated with 1 M LiTFSI in TEGDME as the electrolyte. To determine the stability of the LiTFSI/TEGDME electrolyte, we ran a blank test determining the current−voltage response of the cell using the Co_3Mo_3N as electrode. Figure S6 (Supporting Information) shows the results, demonstrating that the TEGDME electrolyte began to decompose at over 4.3 V and significantly increase over 4.5 V. To alleviate electrolyte decomposition during charge, we constrained the charge potential to 4.3 V (below the electrolyte decomposition region).[17−22] Parts a and b of Figure 4 show the discharge−

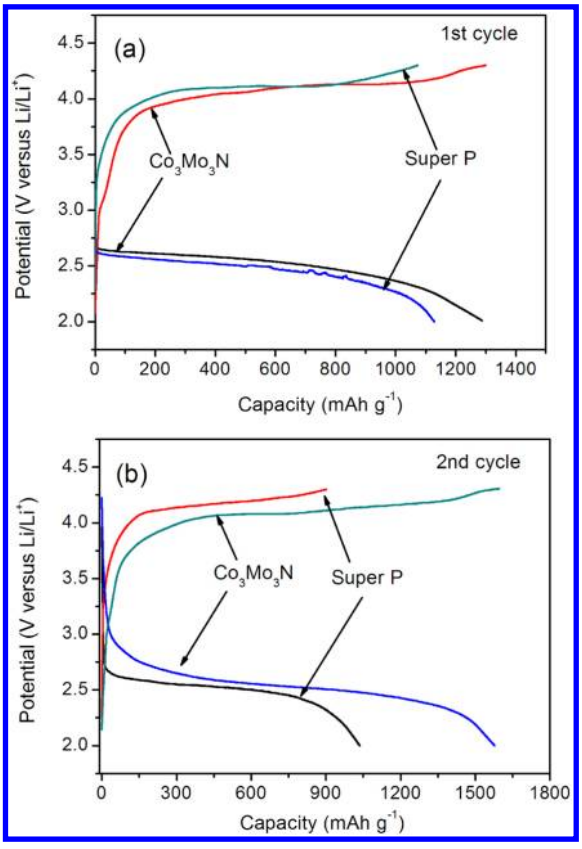

Figure 4. Li−O_2 cell discharge/charge profiles of super P and Co_3Mo_3N-based electrodes in TEGDME electrolyte containing 1 M LiTFSI at the current density of 0.1 mA cm^{-2} for (a) the first cycle and (b) the second cycle.

charge profiles of first and second cycles of the Li−O_2 cells. In the voltage window 2.0−4.3 V, the performances of the Li−O_2 cells with Co_3Mo_3N-based electrode and with pure super P electrode were compared at the same current density (0.1 mA cm^{-2}) in 1 M LiTFSI/TEGDME electrolyte. It can be found that the discharge and charge voltages of Li−O_2 cells can be influenced by Co_3Mo_3N. The discharge voltage of Co_3Mo_3N-based Li−O_2 cell is consistently higher than that of pure carbon-based Li−O_2 cell, and the charge voltage is lower than that of pure carbon-based Li−O_2 cell. This result indicates that Co_3Mo_3N lower the overpotential of discharge/charge process, and therefore confirms the catalytic effect of Co_3Mo_3N in Li−O_2 cells. Presumably, the ORR catalytic activity of Co_3Mo_3N leads to the promoted formation of discharing product near active site of catalyst, followed by the formation on carbon surface. Therefore, the Co_3Mo_3N-based Li−O_2 cell exhibits a higher discharing voltage than pure carbon-based Li−O_2 cell. The charging behavior of Co_3Mo_3N-based Li−O_2 cell should really be consisted of the contribution from both catalytically decomposition of discharing product near active site of Co_3Mo_3N and routine decomposition on carbon surface reactions.[39] The catalytic promoted reaction near active site of Co_3Mo_3N should occur first due to a lower reaction barrier, followed by the decomposition reaction on carbon surface. It should be the reason that the cell with Co_3Mo_3N catalyst showed a lower overpotential than that with only super P material during cycling.

The discharge and charge voltage profiles of the Co_3Mo_3N-based electrode at various cycles at a current density of 0.1 mA cm^{-2} in the voltage windows between 2.0 and 4.3 V is presented in Figure 5. The discharge capacity of the Co_3Mo_3N-

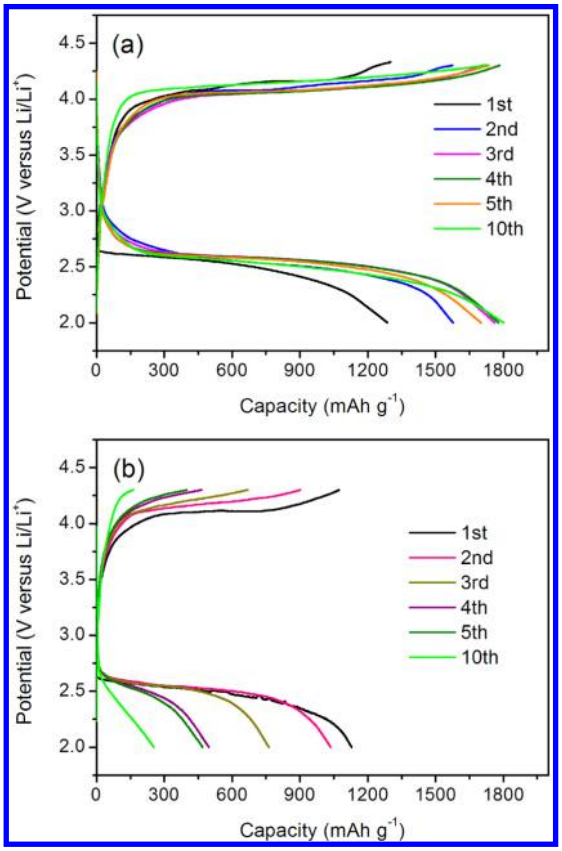

Figure 5. (a) Discharge and charge voltage profiles of the Co_3Mo_3N-based cell at various cycles at a current density of 0.1 mA cm^{-2} in the voltage windows between 2.0 and 4.3 V. (b) Discharge and charge voltage profiles of the super P-based cell at various cycles at a current density of 0.1 mA cm^{-2} in the voltage windows between 2.0 and 4.3 V.

based Li−O_2 battery stabilizes above 1670 mAh g^{-1} on the subsequent 16 cycles at a deep discharge to 2.0 V (Figure 5a). By contrast, the initial discharge capacity of Li−O_2 battery with pure super P cathode is 1150 mAh g^{-1}, and it dramatically drops to 100 mAh g^{-1} after the 15th cycling (Figure 5b and Figure S7, Supporting Information). It can be seen that both the discharge and charge plateaus of Co_3Mo_3N-based Li−O_2 battery are well preserved upon cycling in the voltage window between 2.0 and 4.3 V. This is quite different from most reported tests by restricting capacity to reach good reversibility, in which the control of the discharge/charge capacity was used to avoid the electrolyte decomposition and the deep discharge state of the oxygen electrode.[6,19,20,33] The Co_3Mo_3N-based Li−

dx.doi.org/10.1021/jp310571y | J. Phys. Chem. C 2013, 117, 858−865

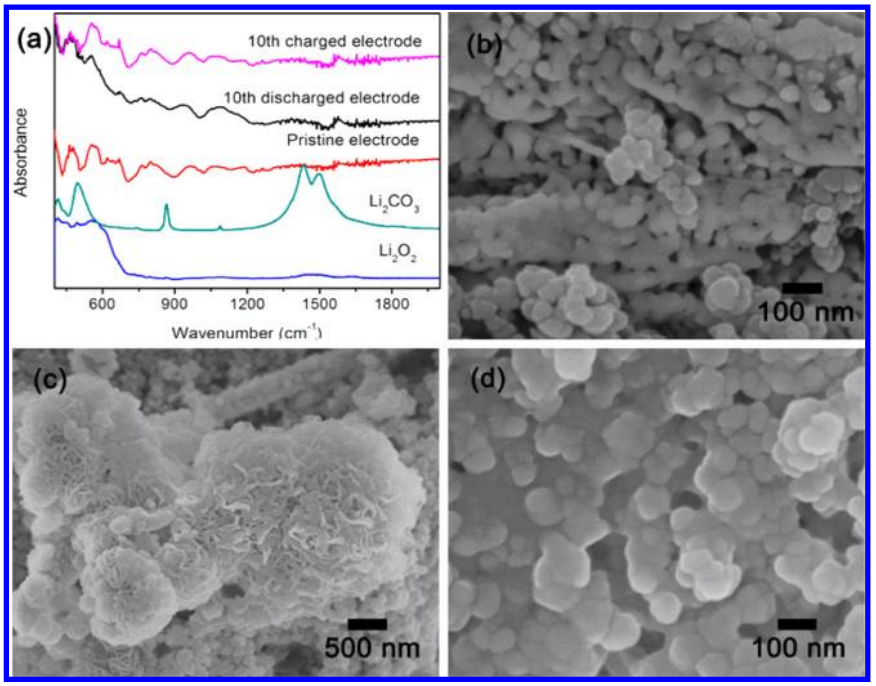

Figure 6. (a) FTIR spectra of Co_3Mo_3N-based cathode at the 10th discharge and recharge. SEM images before 1st discharge (b), after 1st discharge, (c) and after 1st recharge state (d) of Co_3Mo_3N-based cathode.

O_2 battery was found to exhibit an increasing capacity in early three cycles owing to a gradual activation mechanism which was favorable for the improvement of electrochemical kinetics. Nazar et al reported that as a good ORR catalyst, carbon was not effective for OER.[40] Bruce et al demonstated that the carbon reacted with Li_2O_2 on charge cycle to produce an interfacial layer of Li_2CO_3, which increased the OER overpotential.[39] From Figure 4 and Figure 5, it can be found that for the super P-based Li−O_2 cell, the overpotential of second charging curve increased apparently than that of first cycle. This phenomenon is in agreement with the above-mentioned reports, which involves carbon corrosion that permanently modifies the carbon surface. However, due to the good stability of metallic compounds during charging, the Co_3Mo_3N catalyst still remains their catalytic activity after first cycle. Therefore, in the second and subsequent cycles the Co_3Mo_3N catalyst works much better than carbon, resulting in almost unchanged overpotentials and much improved cycle stability.

XRD analysis of the discharged products showed the formation of crystalline Li_2O_2 (Figure S8, Supporting Information), which is agreement with previous studies when ether-based electrolytes were used in Li−O_2 batteries.[5,6] The discharged and recharged electrodes after 10th cycle were also studied by FTIR spectroscopy. Because there is an obvious peak overlap between the pristine Co_3Mo_3N electrode and Li_2O_2, it is hard to identify the existence of Li_2O_2 from the discharged electrode. There is no peak overlap between the pristine electrode and Li_2CO_3, therefore, the absence of Li_2CO_3 characteristic signals in the discharged electrode implies that the product was not Li_2CO_3. The discharge−charge behavior was further examined by SEM. Before discharge, the mesoporous Co_3Mo_3N and Super P carbon nanoparticles are observed in the as-prepared cathode (Figure 6b). After discharge, many close-packed nanosheets are observed on the surface of cathode, which are considered as aggregates comprised of nanocrystalline Li_2O_2 (Figure 6c).[41] After charge, a relatively clean cathode is observed. These Li_2O_2 nanosheets are invisible, but some residual amorphous films remain, which should be due to the Li_2O_2 decomposition during charge (Figure 6d). In addition, TEM image shows that Co_3Mo_3N still maintains the mesoporous structure after cycling (Figure S9, Supporting Information), which illustrates its good structure stability. Solvent stability after the 16th cycle was tested using ^1H and ^{13}C NMR (Figures S10 and S11, Supporting Information), which indicate that TEGDME electrolyte may suffer from minor reactivity on cycling in our case. Thus, Li_2O_2 formation/dissolution was confirmed by SEM after discharge/charge, meanwhile the accumulatation of irreversible electrolyte decomposition product was also observed after recharge.[42]

The high performance of the Co_3Mo_3N catalyst should be attributed to its high electrocatlytic activity afforded by their inherently electronic structure and good electron transport. It has been reported that $NiMoN_x$ possesses an electron-donating ability to enhance its catalytic by XANES.[28] Since Co_3Mo_3N is also a transition bimetallic nitrides and Co belongs to the same group as Ni, the same electron-donating effect may also exist with Co_3Mo_3N, resulting in the favorable electronic structure of Co_3Mo_3N and thus the intrinsic high electrocatlytic activity. In addition, the mesoporous structure of Co_3Mo_3N should also play an important role in its catalytic behavior. This mesoporous structure can not only provide enough void volume for Li_2O_2 deposition, but also promote the flow of oxygen and infiltration of the electrolyte, and eventually improve the capacity and cyclability greatly. The advantageous combination of the intrinsically high catlaytic activity and the unique structure is responsible for the superior performance of the Co_3Mo_3N-based Li−O_2 batteries.

The electrochemical performance of Co_3Mo_3N catalyst for the discharge reaction of the Li−O_2 batteries (Figure 5) was consistent with the ORR activity behavior measured in both nonaqueous (Figure 3d) and aqueous electrolytes (Figure 3a). However, it seems that the catalytic capability for the charging

dx.doi.org/10.1021/jp310571y | J. Phys. Chem. C 2013, 117, 858−865

reaction in nonaqueous electrolyte was not directly correlated with the OER activity in aqueous solutions (Figure 3c). The catalytic behavior for OER is one of the major challenges in rechargeable Li−O_2 batteries, because the electrochemical decomposition of the solid discharge product involves a large anodic polarization. In this work, the introduction of Co_3Mo_3N could catalyze the decomposition of the reaction product. The charge potential increase in cycling owes to mass transport issues and arising from the lowered discharge electrodeposit conductivity and some electrolyte oxidation at higher potential required for charge. This finding provides an evidence that Co_3Mo_3N can catalyze the discharge product at least to a certain degree during the early cycles in LiTFSI/TEGDME electrolyte. The high charge−discharge efficiency and good cycle stability was obtained in the LiTFSI/TEGDME electrolyte owing to a stable interface between optimized electrolyte and electrode material. Although novel electrolytes need to be further explored for better cycling performance, Co_3Mo_3N exhibits promising performances in different electrolytes and can be highly desirable as an alternative cathode for Li−O_2 battery.

CONCLUSIONS

In summary, mesoporous Co_3Mo_3N was prepared by a coprecipitation method followed by ammonia treatment. The obtained Co_3Mo_3N displays excellent bifunctional electrocatalytic activity for ORR/OER in alkaline solution. When Co_3Mo_3N is applied as cathode catalyst, the assembled Li−O_2 battery shows promising discharge capacity and cycling stability. The good performance of the assembled Li−O_2 battery is attributed to the intrinsically electronic structure, inherently high electrocatalytic activities and mesoporous structure of Co_3Mo_3N. The results demonstrate that Co_3Mo_3N is a promising bifunctional catalyst material for Li−O_2 battery application. This work should aid the rational design and facile preparation of novel transition bimetallic nitrides based electrocatalysts to guide the development of Li−O_2 batteries and fuel cells.

ASSOCIATED CONTENT

Supporting Information

Experimental details and additional supporting figure. This material is available free of charge via the Internet at http://pubs.acs.org.

AUTHOR INFORMATION

Corresponding Author

*E-mail: cuigl@qibebt.ac.cn.

Author Contributions

‖These authors contributed equally to this work.

Notes

The authors declare no competing financial interest.

ACKNOWLEDGMENTS

This work was supported by the key Research Program of the Chinese Academy of Sciences. Grant No. KGZD-EW-202-2, “100 Talents” program of Chinese Academy of Sciences, National Program on Key Basic Research Project of China (No. MOST2011CB935700), National Natural Science Foundation of China (Grant No. 20971077, and 21275151), Shandong Province Fund for Distinguished Young Scientist (JQ200906), and Doctoral Fund of Shandong Province (BS2012NJ011).

REFERENCES

(1) Abraham, K. M.; Jiang, Z. *J. Electrochem. Soc.* **1996**, *143*, 1−5.
(2) Girishkumar, G.; McCloskey, B.; Luntz, A. C.; Swanson, S.; Wilcke, W. *J. Phys. Chem. Lett.* **2010**, *1*, 2193−2203.
(3) Peng, Z. Q.; Freunberger, S. A.; Chen, Y. H.; Bruce, P. G. *Science* **2012**, *337*, 563−566.
(4) Shao, Y. Y.; Park, S.; Xiao, J.; Zhang, J. G.; Wang, Y.; Liu, J. *ACS Catal.* **2012**, *2*, 844−857.
(5) Oh, S. H.; Nazar, L. F. *Adv. Energy Mater.* **2012**, *2*, 903−910.
(6) Jung, H. G.; Hassoun, J.; Park, J. B.; Sun, Y. K.; Scrosati, B. *Nat. Chem.* **2012**, *4*, 579−585.
(7) Jung, K. N.; Lee, J. I.; Im, W. B.; Yoon, S.; Shina, K. H.; Lee, J. W. *Chem. Commun.* **2012**, *48*, 9406−9408.
(8) Park, M.; Sun, H.; Lee, H.; Lee, J.; Cho, J. *Adv. Energy Mater.* **2012**, *2*, 780−800.
(9) Cui, Y. M.; Wen, Z. Y.; Liu, Y. *Energy Environ. Sci.* **2011**, *4*, 4727−4734.
(10) Lu, Y. C.; Xu, Z. C.; Gasteiger, H. A.; Chen, S.; Schifferli, K. H.; Yang, S. H. *J. Am. Chem. Soc.* **2010**, *132*, 12170−12171.
(11) Thapa, A. K.; Hidaka, Y.; Hagiwara, H.; Ida, S.; Ishihara, T. *J. Electrochem. Soc.* **2011**, *15*, A1483−1489.
(12) Wang, H. L.; Yang, Y.; Liang, Y. Y.; Zheng, G. Y.; Li, Y. G.; Cui, Y.; Dai, H. J. *Energy Environ. Sci.* **2012**, *5*, 7931−7935.
(13) Wang, L.; Zhao, X.; Lu, Y. H.; Xu, M. W.; Zhang, D. W.; Ruoff, R. S.; Stevenson, K. J.; Goodenough, J. B. *J. Electrochem. Soc.* **2011**, *158*, A1379−1382.
(14) Freunberger, S. A.; Chen, Y.; Peng, Z.; Griffin, J. M.; Hardwick, L. J.; Barde, F.; Novak, P.; Bruce, P. G. *J. Am. Chem. Soc.* **2011**, *133*, 8040−8047.
(15) Black, R.; Oh, S. H.; Lee, J. H.; Yim, T.; Adams, B.; Nazar, L. F. *J. Am. Chem. Soc.* **2012**, *134*, 2902−2905.
(16) Débart, A.; Paterson, A. J.; Bao, J.; Bruce, P. G. *Angew. Chem., Int. Ed.* **2008**, *47*, 4521−4524.
(17) McCloskey, B. D.; Scheffler, R.; Speidel, A.; Bethune, D. S.; Shelby, R. M.; Luntz, A. C. *J. Am. Chem. Soc.* **2011**, *133*, 18038−18041.
(18) Zhang, L. L.; Zhang, X. B.; Wang, Z. L.; Xu, J. J.; Xu, D.; Wang, L. M. *Chem. Commun.* **2012**, *48*, 7598−7600.
(19) Lim, H. D.; Park, K. Y.; Gwon, H.; Hong, J.; Kim, H.; Kang, K. *Chem. Commun.* **2012**, *48*, 8374−8376.
(20) Wang, Z. L.; Xu, D.; Xu, J. J.; Zhang, L. L.; Zhang, X. B. *Adv. Funct. Mater.* **2012**, *22*, 3699−3705.
(21) Shao, Y. Y.; Ding, F.; Xiao, J.; Zhang, J.; Xu, W.; Park, S.; Zhang, J. G.; Wang, Y.; Liu, J. *Adv. Funct. Mater.* **2012**, DOI: 10.1002/adfm.201200688.
(22) Freunberger, S. A.; Chen, Y. H.; Drewett, N. E.; Hardwick, L. J.; Bardé, F.; Bruce, P. G. *Angew. Chem., Int. Ed.* **2011**, *50*, 8609−8613.
(23) Kenichiro, H.; Masatoshi, N.; Shinzo, O. *J. Phys. Chem. B* **2001**, *105*, 4084−4093.
(24) Ramanathan, S.; Yu, C. C.; Oyama, S. T. *J. Catal.* **1998**, *173*, 10−16.
(25) Milad, I. K.; Smith, K. J.; Philip, C. W.; Mitchell, A. R. *Catal. Lett.* **1998**, *52*, 113−119.
(26) Cardona, C. M.; Elliott, B.; Echegoyen, L. *J. Am. Chem. Soc.* **2006**, *128*, 6480−6485.
(27) Prior, T. J.; Battle, P. D. *J. Mater. Chem.* **2004**, *14*, 3001−3007.
(28) Chen, W. F.; Sasaki, K.; Ma, C.; Frenkel, A. I.; Marinkovic, N.; Muckerman, J. T.; Zhu, Y.; Adzic, R. R. *Angew. Chem. Int, Ed.* **2012**, *51*, 6031−6035.
(29) Cong, Y.; Park, H. S.; Dang, H. X.; Fan, F. R. F.; Bard, A. J.; Mullins, C. B. *Chem. Mater.* **2012**, *24*, 579−586.
(30) Hunter, S. M.; McKay, D.; Smith, R. I.; Hargreaves, J. S. J.; Gregory, D. H. *Chem. Mater.* **2010**, *22*, 2898−2907.
(31) McKay, D.; Gregory, D. H.; Hargreaves, J. S. J.; Hunter, S. M.; Sun, X. *Chem. Commun.* **2007**, *29*, 3051−3053.
(32) Kojima, R.; Aika, K. I. *Appl. Catal., A* **2001**, *219*, 157−170.
(33) Jacobsen, C. J. H.; Dahl, S.; Clausen, B. S.; Bahn, S.; Logadottir, A.; Norskov, J. K. *J. Am. Chem. Soc.* **2001**, *123*, 8404−8405.

(34) Dong, S. M.; Chen, X.; Zhang, K. J.; Gu, L.; Zhang, L. X.; Zhou, X. H.; Cui, G. L.; Chen, L. Q. *Chem. Commun.* **2011**, *47*, 11291−11293.
(35) Qi, J.; Jing, L. H.; Jiang, Q.; Wang, S. L.; Sun, G. Q. *J. Phys. Chem. C* **2010**, *114*, 18159−18166.
(36) Hamdani, M.; Singh, R. N.; Chartier, P. *Int. J. Electrochem. Sci.* **2010**, *5*, 556−577.
(37) Shui, J. L.; Karan, N. K.; Balasubramanian, M.; Li, S. Y.; Liu, D. J. *J. Am. Chem. Soc.* **2012**, *134*, 16654−16661.
(38) Laoire, C. O.; Mukerjee, S.; Abraham, K. M. *J. Phys. Chem. C* **2010**, *114*, 9178−9186.
(39) Peng, Z. Q.; Freunberger, S. A.; Hardwick, L. J.; Chen, Y.; Giordani, V.; Bardé, F.; Novák, P.; Graham, D.; Tarascon, J. M.; Bruce, P. G. *Angew. Chem., Int. Ed.* **2011**, *50*, 6351−6355.
(40) Black, R.; Lee, J. H.; Adams, B.; Mims, C. A.; Nazar, L. F. *Angew. Chem., Int. Ed.* **2013**, *52*, 392−396.
(41) Li, Y. L.; Wang, J. J.; Li, X. F.; Geng, D. S.; Banis, M. N.; Tang, Y. J.; Wang, D. N.; Sun, X. L. *J. Mater. Chem.* **2012**, *22*, 20170−20174.
(42) Oh, S. H.; Black, R.; Pomerantseva, E.; Lee, J. H.; Nazar, L. F. *Nat. Chem.* **2012**, *4*, 1004−1010.